Acta Biomaterialia 6 (2010) 3583–3594

Contents lists available at ScienceDirect

Acta Biomaterialia

journal homepage: www.elsevier.com/locate/actabiomat

Raman tensor analysis of ultra-high molecular weight polyethylene and its application to study retrieved hip joint components

Yasuhito Takahashi, Leonardo Puppulin, Wenliang Zhu, Giuseppe Pezzotti *

Ceramic Physics Laboratory & Research Institute for Nanoscience, RIN, Kyoto Institute of Technology, Sakyo-ku, Matsugasaki, 606-8585 Kyoto, Japan

ARTICLE INFO

Article history:
Received 7 August 2009
Received in revised form 26 February 2010
Accepted 26 February 2010
Available online 6 March 2010

Keywords:
Raman tensor elements
Polarized Raman analysis
UHMWPE
Molecular orientation
Acetabular cups

ABSTRACT

The angular dependences of the polarized Raman intensity of A_g, B_{1g}, B_{2g}, and B_{3g} modes have been preliminary investigated on a model fiber sample of ultra-high molecular weight polyethylene (UHMWPE) in order to retrieve the Raman tensor elements, i.e. the intrinsic parameters governing the vibrational behavior of the orthorhombic structure of polyethylene. Based on this Raman analysis, a method is proposed for determining unknown crystallographic orientation patterns in UHMWPE biomedical components concurrently with the orientation distribution functions for orthorhombic lamellae. An application of the method is shown, in which we quantitatively examined the molecular orientation patterns developed on the surface of four in vivo exposed UHMWPE acetabular cups vs. an unused cup. Interesting findings were: (i) a clear bimodal distribution of orientation angles was observed on worn surfaces; and (ii) a definite and systematic increase in both molecular orientation and crystallinity in main wear zones vs. non-wear zones was found in all retrieved acetabular cups. The present crystallographic analysis is an extension of our previous Raman studies of UHMWPE acetabular cups related to assessments of oxidation and residual strain and suggests a viable path to track back wear-history information from the surface of UHMWPE, thus unfolding the in vivo kinematics of the bearing surfaces in hip joints on the microscopic scale.

1. Introduction

The most widely used type of prosthesis in total hip arthroplasty (THA) consists of a system with a femoral head made of a metal alloy (e.g. CoCr) impinging against an ultra-high molecular weight polyethylene (UHMWPE) acetabular cup. In this hip joint system, the UHMWPE acetabular cup undertakes the multiple roles of body-weight bearing, low-friction sliding surface, and impact absorber. Accordingly, it is liable to experience extensive creep and wear damages with the concurrent formation of polyethylene debris, which eventually leads to joint loosening and osteolysis (i.e. to the need for further surgery) [1,2]. In other words, UHMWPE components unavoidably degrade both chemically and mechanically during in vivo implantation. In an attempt to both clarify the origin of implant degradation and propose methods for elongating their lifetime, a number of Raman studies have been carried out, focusing on phenomena of chemical and structural degradation (e.g. oxidation and degree of crystallinity) in the polyethylene structure [3–7]. On the other hand, Raman measurements of residual strain in UHMWPE acetabular cups have provided an effective tool for the quantitative assessment of mechanical degradation in terms of residual strain [8,9]. In particular, this latter Raman spectroscopic method provided us with an experimental path to separate creep and wear contributions from the dimensional change experimentally observed in in vivo exposed acetabular cups. Although Raman studies of chemical, structural, and mechanical alterations have greatly contributed to advancing our knowledge of degradation processes in biomedical UHMWPE grades, there is still a long way to go before the development of a rigorous in vivo lifetime prediction of biomedical components becomes available. The reason for such a lack of information might partly reside in the fact that additional structural factors (i.e. besides crystallinity) are often not considered to be as important as the chemical and mechanical ones: the occurrence of local crystallographic alignment of the polyethylene lamellae. Polarized Raman spectroscopy possesses the potential to quantitatively unfold the missing crystallographic information by screening with a laser microprobe the molecular orientation patterns developed on the surface of acetabular components [10–15]; however, such an evaluation represents a formidable experimental and computational task. Crystalline (e.g. mainly orthorhombic) phases in UHMWPE might be randomly oriented within the amorphous matrix or be preferentially oriented as a consequence of the manufacturing pro-

* Corresponding author. Tel./fax: +81 75 724 7568.
E-mail address: pezzotti@kit.ac.jp (G. Pezzotti).

1742-7061/$ - see front matter © 2010 Acta Materialia Inc. Published by Elsevier Ltd. All rights reserved.
doi:10.1016/j.actbio.2010.02.051

cess. However, the orientation of crystalline lamellae is sensitive to mechanical and frictional loading [16–18]. Therefore, the lamellae will unavoidably tend to preferentially orient themselves on the surface of UHMWPE acetabular cup during in vivo loading. This molecular re-arrangement reflects both primary and secondary motions generated at the contact surface in artificial hip joints, thus representing an important mechanism, precursor to the formation of wear debris throughout the loading history.

In this paper, we have focused on the determination of a spectroscopic method aimed at quantifying the degree of molecular orientation and the angular distributions of orthorhombic lamellae on the surface of UHMWPE. Preliminary to such assessments, we made efforts in explicitly describing the Raman selection rules and in experimentally calibrating the relevant Raman tensor elements intrinsic to the orthorhombic structure of polyethylene using a model sample (i.e. an UHMWPE fiber with almost totally aligned molecular structure). An additional step has then been that of introducing an orientation distribution function (i.e. formulated from Wigner functions in terms of Legendre polynomials [19–21]) into the mathematical algorithm of Raman crystallographic orientation analysis, with the ultimate goal of quantifying the local degree of alignment of the structure concurrently to the orientation in space of the *c*-axis of the orthorhombic cell. According to the knowledge of both intrinsic vibrational parameters and orientation distribution functions, we could quantitatively discuss the orientation of orthorhombic lamellae from relative changes in intensity of selected Raman bands in both parallel and cross polarization geometries. The structure of the paper is organized as follows. Section 2 briefly describes the UHMWPE material used for Raman calibrations, the unused and retrieved samples from hip joint surgeries, as well as the salient technical aspects of our confocal/polarized Raman equipment. Section 3, which also contains a brief description of the Raman bands of the orthorhombic UHMWPE structure, is mainly dedicated to theoretical analyses of the Raman intensity dependences on molecular orientation and to the explicit description of the role of orientation distribution functions in the Raman selection rules of an orthorhombic polyethylene structure. This section ends with establishing the working equations that describe the orientation distribution function and the Raman selection rules in terms of three Euler angles, thus locating the *c*-axes of orthorhombic lamellae in space with respect to the sample surface. In Section 4, we apply the polarized Raman scattering technique to quantitatively describe the orientation patterns generated in four acetabular cups retrieved after different periods of in vivo exposure (ranging between about 2 and 12 years of exposure time in vivo). Areas from main wear and non-wear zones are characterized in comparison to an unused acetabular cup, and a brief discussion is offered in comparison with crystallinity data collected at the same studied locations. In Section 5 we present our conclusions.

2. Materials and methods

2.1. UHMWPE fiber for Raman tensor calibration

The UHMWPE fiber used for spectroscopic calibrations was a commercially available sample manufactured by Ningbo Dancheng Advanced Materials Co. Ltd. (Zhejiang, China). This fiber, typically ≈25 μm in diameter, possessed a high molecular weight (approx. three million), interlinking, high degree of uniaxial orientation and high crystallinity. According to the X-ray diffraction measurements provided by the manufacturer, the orthorhombic cell is prevalent in the structure with its *c*-axis being strongly oriented along the long axis of the fiber. This point will be further clarified in the quantitative Raman analysis of the degree of molecular orientation shown in the remainder of this paper. A draft of the orthorhombic cell and its average orientation with respect to the fiber structure is shown in Fig. 1a. Our Raman analysis also clarified that, as far as the rotation angle around the long axis of the fiber is concerned, the investigated UHMWPE fiber experienced a domain-like structure in the *c*-plane, each domain experiencing constant in-plane angle. The size of the domains was typically in the order of few cubic μm, namely of a size comparable with our confocal Raman probe (cf. Section 2.3 below). Such a peculiar microstructure of the fiber sample, already reported by other authors [22], was the key factor in locating the intrinsic vibrational characteristics of an UHMWPE orthorhombic crystal cell.

2.2. Unused and retrieved UHMWPE acetabular cups

Four different acetabular cups were investigated, which were all retrieved from left-side hip joints in the respective patient bodies at Tokyo Medical University. These acetabular cups will also be referred to as short-term (2.4- and 2.8-year) and long-term (10.3- and 12.2-year) retrievals, respectively. The short-term retrieved acetabular components were both made of highly cross-linked polyethylene, manufactured from 1900H bar stock by isostatic compression molding (with no addition of calcium stearate) (ArCom®, Biomet Japan Inc., Tokyo, Japan) and sterilized by γ-ray irradiation with a dose of 33 kGy. One cup belonged to a 61 year old male patient for which the cause of revision was infection with a follow-up period of 2.4 years, while the other cup belonged to a 53 year old female patient for which the cause of revision was infection dislocation with a follow-up period of 2.8 years. On the other hand, two long-term retrievals were made from GUR4150 bar stock by Ram extraction molding (calcium stearate was added in these case) and sterilized with a dose of γ-ray radiation ranging between 25 and 37 kGy. One cup (manufactured by Zimmer Inc., Tokyo, Japan) belonged to a 47 year old male patient, while the other cup (ArCom®, Biomet Japan Inc., Tokyo, Japan) belonged to a 60 year old female patient. Both cups were retrieved due to aseptic loosening and the follow-up period was 10.4 and 12.2 years, respectively.

For comparison, an unused acetabular cup was investigated, which was also from the Biomet manufacturer and possessed the same manufacturing characteristics of the short-term retrieval described above. Locating the main wear zone on both short-term and long-term retrievals could be pursued in a relatively easy way by the naked eye, owing to a slight difference in surface roughness (and thus in sample translucency) as compared to the non-wear zone. On the other hand, an exception was the short-term retrievals exposed in vivo for 2.8 years, for which such an observation was difficult. In this latter case, we assumed the main wear zone to be located within the angular interval 30–40° from the location of cup dome, in analogy with the other retrievals studied.

2.3. Polarized Raman spectroscopy

Raman spectra were collected at room temperature with a triple-monochromator (T-64000, HORIBA/Jobin–Yvon, Kyoto, Japan) equipped with a charge-coupled device (CCD) detector. Spectral analyses were performed by means of commercially available software (Labspec, HORIBA/Jobin–Yvon, Kyoto, Japan). The laser excitation source was a monochromatic blue line emitted by an Ar-ion laser at a wavelength of 488 nm (Stabilite 2017, Spectra Physics, Mountain View, CA) with a power of 100 mW. The integration time for acquiring a spectrum (namely at each pixel of the collected Raman maps) was typically 15 s. Preliminary experiments were made for checking about the possibility of heating effects on the sample by laser irradiation. The outcome of such experiments

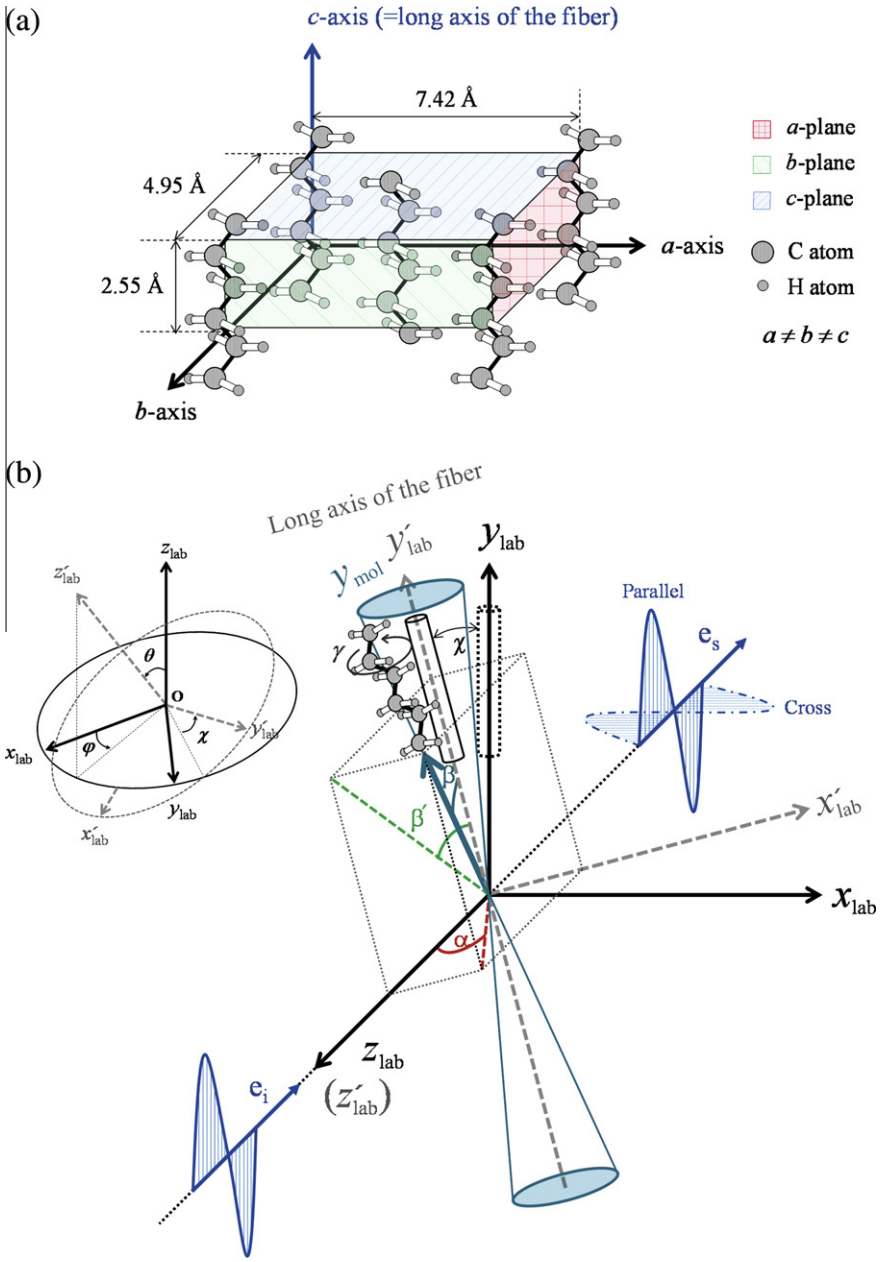

Fig. 1. Choice of Euler rotation angles and Cartesian coordinates: (a) with respect to the orthorhombic structure of UHMWPE, and (b) with respect to the axis of preferential orientation in the fiber sample).

showed that detectable alterations of the Raman spectrum of UHMWPE started after laser exposures as long as 45 min, which is much longer than the exposure time needed in the present measurements. The confocal configuration of the probe adopted throughout the present experiment corresponded to a 100× objective lens; numerical objective aperture, confocal pinhole diameter, and focal length of the objective lens were fixed as: NA = 0.9, Φ = 100 μm and f = 11 mm, respectively. The size of the confocal probe focused on the sample surface was quantitatively calibrated in a previous study [23] as 2.2 and 6.4 μm in diameter and depth, respectively. In that study, the confocal probe response could be expressed according to the following function [24]:

$$B(z, z_0) = \exp(-2\alpha z)\frac{p^2}{p^2 + (z - z_0)^2} \quad (1)$$

with z and z_0 being the in-depth abscissa of the point from which the Raman light is scattered and that of the focal point, respectively, while the parameters p and α were experimentally retrieved as 2.4 μm and 0.04 m^{-1}, respectively. In both cases of Raman experiments on fiber and acetabular cup samples, the probe was focused at the surface of the sample. Owing to the relatively small size of the probe as compared with the diameter of the fiber, no correction for probe configuration was made in comparing experiments on fiber and acetabular cups.

A rotation jig was employed for calibrating the angular dependence of selected Raman bands as collected on the UHMWPE fiber sample. Fig. 1b shows a schematic draft of the definition of rotation angle, χ (i.e. belonging to a set of three Euler angles (θ, φ, χ) defined with respect to our choice of Cartesian axes), adopted for this calibration. The fiber was placed on the rotating jig with its long axis parallel to the polarization direction of the incident laser beam. Spectra were recorded through the parallel or cross polarization filters, which were set to pass the scattered Raman radiation horizontally or vertically to a CCD camera. This procedure was re-

peated with rotating the fiber (i.e. the *c*-axis of the orthorhombic structure) from 0° to 180° by incremental steps of 5°. According to this procedure, calibration curves of Raman intensity as a function of rotation angle could be obtained from the two selected polarization geometries, which were fitted to continuous functions using commercially available software (Mathematica 4; Wolfram Research Inc., IL, USA). Raman spectral mapping was performed in both parallel and cross polarization geometries in order to characterize orientation patterns on wear and non-wear zones of four retrieved acetabular cups and, for comparison, on an unused cup. Owing to the convex character of the investigated surfaces and the need for keeping in focus the mapped surface, an upper limit on the size of a Raman map was typically 100 × 100 μm in dimension (i.e. with a sampling of 5 μm step for a total of 21 × 21 = 441 points). However, in order to secure an acceptable degree of statistical reliability in representing the molecular arrangement in the selected zone of a cup, mapping was repeated at 5 random locations of each selected zone for each individual cup (i.e. ≈10^5 μm^2 per each investigated cup). The obtained maps of relative Raman intensity were then converted into maps (and histograms) of average molecular orientation (according to the quantitative knowledge of the Raman tensor elements) and maps (and histograms) of degree of crystallinity as well. Furthermore, the orientation distribution functions obtained for non-wear and main wear zones were determined and compared with that of the unused cup. The total number of collected Raman spectra on all the retrievals (including both main wear and non-wear zones, and angular rotations at each point) and the fiber sample used for calibration was in the order of 10^5 for a total measurement time of ≈1100 h.

3. Theoretical assessments

3.1. Raman bands from the UHMWPE structure and its crystallinity assessment

The relationship between the observed Raman bands and the vibrational modes of the orthorhombic polyethylene structure is amply documented in the pre-existing literature [9,10]. Briefly here, we summarize the main features found in the Raman spectrum of UHMWPE in the 1000–1500 cm^{-1} spectral region, which are also explicitly listed in Table 1. The spectrum can be subdivided into three main regions: region (I) in the interval 1000–1200 cm^{-1}, which is dominated by C–C stretching vibrations; region (II) at around 1300 cm^{-1}, which is dominated by $–CH_2–$ twisting vibrations; and, region (III) in the interval 1400 and 1500 cm^{-1}, which is dominated by $–CH_2–$ wagging vibrations. In dealing with a highly crystallized structure, as in the case of the fiber sample, the vibrations with tensor axis coincident with the axes of the crystalline orthorhombic units are expected to contribute the most relevant part of the detected Raman intensity. In other words, the modes with A_g, B_{2g}, and B_{3g} symmetry, which satisfy this requirement, should have a dominating effect on the polarized Raman spectra of the UHMWPE structure studied here as compared with the B_{1g} mode (i.e. mainly related to the amorphous structure). Two broad bands located at 1080 and 1310 cm^{-1} are also assigned to the amorphous (matrix) phase. In the case of all the UHMWPE samples investigated here, the intensities of these bands were conspicuously weak (and vanishingly low in the fiber sample) as a consequence of a high degree of crystallinity and highly aligned molecular structure. Nevertheless, we have assessed the degree of crystallinity using the relative intensity of the band located at 1296 cm^{-1} (representing the crystalline part of the structure) vs. the band located at 1310 cm^{-1} (representing the amorphous structure), according to the equation given by Mutter et al. [25], as follows:

$$\alpha_c = \frac{I_{1296}}{I_{1296} + I_{1310}} \tag{2}$$

where I is the integral intensity of the Raman band (i.e. collected in a non-polarized configuration) whose wavenumber is identified by the subscript.

The band located at 1170 cm^{-1} possesses $A_g + B_{1g}$ symmetry and results from the CH_2 rocking mode. The 1130 cm^{-1} band, also with $A_g + B_{1g}$ symmetry, mostly arises from the crystalline part of the polymer, but the trans C–C bonds in the amorphous phase are also expected to contribute to the scattering intensity at this frequency. Maxfield et al. [10] have used this band to calculate the orientation of the crystalline part of low-density polyethylene. This band was clearly visible in the Raman spectra of the calibration sample used, but, in the polarization geometries relevant to this study, its intensity was very low and hampered a precise characterization of intensity variations as a function of geometrical rotation. The origin of bands related to CH_2 bending modes at around 1450 cm^{-1} is the most ambiguous in polyethylene because of the possibility of Fermi resonance between the Raman active CH_2 bending modes and its first overtones and the possible combinations of the infrared active CH_2 rocking modes [11]. In addition, combinations with infrared active CH_2 rocking modes cannot be ruled out. All these reasons suggested not selecting bands belonging to CH_2 bending modes for our Raman polarization analyses. Nevertheless, it has been shown that, for orthorhombic polyethylene, which contains two structural units per unit cell, factor group splitting of the CH_2 mode results in the presence of two components at 1418 and 1440 cm^{-1}. Two sharp bands located at 1130 cm^{-1} ($A_g + B_{1g}$) and at 1296 cm^{-1} ($B_{2g} + B_{3g}$), were used throughout the Raman polarization analysis shown in this paper. These bands were clearly visible for any relevant polarization geometry and for any rotation angle of both fiber and acetabular cup samples. The contributions of both B_{1g} and B_{2g} to the intensity of the 1130 and 1296 cm^{-1} bands, respectively, could be neglected in studying the fiber sample because of its very high degree of crystallinity. On the other hand, all the contributing vibrational modes (i.e. A_g, B_{1g}, B_{2g}, and B_{3g} modes) were taken into consideration in assessing the molecular orientation of UHMWPE structures belonging to the acetabular cup in which a non-negligible amount of amorphous phase was present.

Table 1
Raman bands and respective vibrational modes in UHMWPE. Spectral locations are explicitly indicated together with the related phases, vibrational modes and symmetries (in round brackets are the specific molecular species involved with individual vibrational modes).

Wavenumber (cm^{-1})	Phase	Mode	Symmetry
1060	C(A)	ν_{as} (C–C)	$B_{2g} + B_{3g}$
1080	A	ν (C–C)	—
1130	C(A)	ν_s (C–C)	$A_g + B_{1g}$
1170	C(A)	ρ (CH_2)	$A_g + B_{1g}$
1296	C	τ (CH_2)	$B_{2g} + B_{3g}$
1310	A	τ (CH_2)	—
1370	C(A)	ω (CH_2)	$B_{2e} + B_{3g}$
1418	C	σ (CH_2)	A_g
1440	A	σ (CH_2)	$A_g + B_{1g}$
1460	A	σ (CH_2)	$A_g + B_{1g}$

C, crystalline; A, amorphous; ν, stretching (s, symmetric; as, asymmetric); ρ, rocking; σ, bending; τ, twisting; ω, wagging.

3.2. Angular dependence of the polarized Raman spectrum of UHMWPE

The intensity of Raman bands strongly depends on crystal orientation and polarization geometry of the adopted optical configuration, according to the following equation [26]:

$$I \propto |e_i \Re e_s|^2 \tag{3}$$

where I is the scattered Raman intensity, e_i and e_s are the unit polarization vectors of the electric field for incident and scattered light, respectively, and $\Re$ represents the Raman scattering tensor of the particular vibrational mode under consideration. The Raman tensors for the orthorhombic structure are given as [26]:

$$\Re_{A_g}=\begin{vmatrix} a & 0 & 0\\ 0 & b & 0\\ 0 & 0 & c\end{vmatrix},\quad \Re_{B_{1g}}=\begin{vmatrix} 0 & d & 0\\ d & 0 & 0\\ 0 & 0 & 0\end{vmatrix},\quad \Re_{B_{2g}}=\begin{vmatrix} 0 & 0 & e\\ 0 & 0 & 0\\ e & 0 & 0\end{vmatrix},$$
$$\Re_{B_{3g}}=\begin{vmatrix} 0 & 0 & 0\\ 0 & 0 & f\\ 0 & f & 0\end{vmatrix}, \tag{4}$$

where a, b, c, d, e and f are the Raman tensor elements. However, since we are mainly concerned here with $\Re_{A_g}$ and $\Re_{B_{3g}}$, the Raman tensor elements pertaining to the present analysis will only be a, b, c, and f. The dependence of both A_g and B_{3g} modes on the Euler angles (θ, φ, χ) locating the c-axis of the orthorhombic structure in space can be expressed in the laboratory system of Cartesian coordinates, xyz (cf. draft in Fig. 1b), as follows:

$$\Re_{j\ xyz}=\Phi_{xyz}\Re_j\widetilde{\Phi}_{xyz} \tag{5}$$

where the subscript j locates the vibrational mode, while Φ_{xy} and $\widetilde{\Phi}_{xyz}$ are the transformation matrix and its inverse, respectively, given as:

$$\Phi_{xyz}=\begin{pmatrix} \cos\theta\cos\varphi\cos\chi-\sin\varphi\sin\chi & \cos\theta\sin\varphi\cos\chi+\cos\varphi\sin\chi & -\sin\theta\cos\chi\\ -\sin\varphi\cos\chi-\cos\theta\cos\varphi\sin\chi & \cos\varphi\cos\chi-\cos\theta\sin\varphi\sin\chi & \sin\theta\sin\chi\\ \sin\theta\cos\varphi & \sin\theta\sin\varphi & \cos\theta\end{pmatrix} \tag{6}$$

$$\widetilde{\Phi}_{xyz}=\begin{pmatrix} \cos\theta\cos\varphi\cos\chi-\sin\varphi\sin\chi & -\sin\varphi\cos\chi-\cos\theta\cos\varphi\sin\chi & \sin\theta\cos\varphi\\ \cos\theta\sin\varphi\cos\chi+\cos\varphi\sin\chi & \cos\varphi\cos\chi-\cos\theta\sin\varphi\sin\chi & \sin\theta\sin\varphi\\ -\sin\theta\cos\chi & \sin\theta\sin\chi & \cos\theta\end{pmatrix} \tag{7}$$

Note that, in our choice of Euler angles (cf. Fig. 1b), the angle χ represents the in-plane rotation angle, since the plane $(xy)_{\text{lab}}$ corresponds to the plane perpendicular to the back-scattered laser beam. For incident laser polarized along a fixed direction (i.e. the y-axis direction) and scattered light also polarized along the same y-axis (i.e. polarization geometry described as $z(yy)\bar{z}$ in Porto notations [27]), the incident and scattered electric unit vectors can be expressed in Cartesian coordinates xyz, as follows:

$$e^{\parallel}_{i\ xyz}=(0\quad 1\quad 0),\quad e^{\parallel}_{sxyz}=\begin{pmatrix}0\\1\\0\end{pmatrix} \tag{8}$$

where the subscripts i and s refer to incident and scattered light, respectively; and the superscript || refers to the parallel configuration of the polarized probe. On the other hand, when the incident laser is again polarized along the laboratory y-axis direction but the scattered light is along the z-axis (polarization geometry $z(yx)\bar{z}$), the unit electric vectors become:

$$e^{\parallel}_{i\ xyz}=(0\quad 1\quad 0),\quad e^{\perp}_{sxyz}=\begin{pmatrix}1\\0\\0\end{pmatrix} \tag{9}$$

where the superscript $\perp$ locates the choice of a cross-configuration for the polarized probe. Substituting for Eqs. (6)–(8) (or (9)) in Eq. (3), the Raman intensities for A_g, B_{2g}, and B_{3g} modes can be generally expressed as periodic functions of the Raman tensor elements and of three Euler angles in space, as follows:

(i) A_g mode:

$$I^{\parallel}_{A_g}\propto[c\sin^2\theta\sin^2\chi+a(\sin\varphi\cos\chi+\cos\theta\cos\varphi\sin\chi)^2+b(\cos\varphi\cos\chi-\cos\theta\sin\varphi\sin\chi)^2]^2 \tag{10}$$

$$I^{\perp}_{A_g}\propto\left[-\tfrac{1}{2}(a-b)\cos\theta\sin2\varphi\cos2\chi+\sin\chi\cos\chi(a\sin^2\varphi+b\cos^2\varphi-c\sin^2\theta)-\cos^2\theta\sin\chi\cos\chi(a\cos^2\varphi+b\sin^2\varphi)\right]^2 \tag{11}$$

(i) B_{1g} mode:

$$I^{\parallel}_{B_{1g}}\propto[-2d(\sin\varphi\cos\chi+\cos\theta\cos\varphi\sin\chi)(\cos\varphi\cos\chi-\cos\theta\sin\varphi\sin\chi)]^2 \tag{12}$$

$$I^{\perp}_{B_{1g}}\propto[d(\cos\theta\cos2\varphi\cos2\chi-2\cos\varphi\cos\chi\sin\varphi\sin\chi-2\cos^2\theta\cos\varphi\cos\chi\sin\varphi\sin\chi)]^2 \tag{13}$$

(i) B_{2g} mode:

$$I^{\parallel}_{B_{2g}}\propto[-2e\sin\theta\sin\chi(\sin\varphi\cos\chi+\cos\theta\cos\varphi\sin\chi)]^2 \tag{14}$$

$$I^{\perp}_{B_{2g}}\propto[e\sin\theta(\sin\varphi\cos^2\chi-\sin\varphi\sin^2\chi+\cos\theta\cos\varphi\sin2\chi)]^2 \tag{15}$$

(i) B_{3g} mode:

$$I^{\parallel}_{B_{3g}}\propto[2f\sin\theta\sin\chi(\cos\varphi\cos\chi-\cos\theta\sin\varphi\sin\chi)]^2 \tag{16}$$

$$I^{\perp}_{B_{3g}}\propto[f\sin\theta(\cos\theta\sin\varphi\sin2\chi-\cos\varphi\cos2\chi)]^2 \tag{17}$$

For the general structure of UHMWPE, involving both crystalline and amorphous phases, we can retrieve four working equations to describe the intensities of the observed Raman bands, as follows:

$$I^{\parallel}_{A_g+B_{1g}}\propto\alpha_c\left[c\sin^2\theta\sin^2\chi+a(\sin\varphi\cos\chi+\cos\theta\cos\varphi\sin\chi)^2+b(\cos\varphi\cos\chi-\cos\theta\sin\varphi\sin\chi)^2\right]^2+(1-\alpha_c)[-2d(\sin\varphi\cos\chi+\cos\theta\cos\varphi\sin\chi)(\cos\varphi\cos\chi-\cos\theta\sin\varphi\sin\chi)]^2 \tag{18}$$

$$I^{\parallel}_{B_{2g}+B_{3g}}\propto\frac{1}{2}\left\{[-2e\sin\theta\sin\chi(\sin\varphi\cos\chi+\cos\theta\cos\varphi\sin\chi)]^2+[2f\sin\theta\sin\chi(\cos\varphi\cos\chi-\cos\theta\sin\varphi\sin\chi)]^2\right\} \tag{19}$$

$$I^{\perp}_{A_g+B_{1g}}\propto\alpha_c\left[-\frac{1}{2}(a-b)\cos\theta\sin2\varphi\cos2\chi+\sin\chi\cos\chi(a\sin^2\varphi+b\cos^2\varphi-c\sin^2\theta)-\cos^2\theta\sin\chi\cos\chi(a\cos^2\varphi+b\sin^2\varphi)\right]^2+(1-\alpha_c)[d(\cos\theta\cos2\varphi\cos2\chi-2\cos\varphi\cos\chi\sin\varphi\sin\chi-2\cos^2\theta\cos\varphi\cos\chi\sin\varphi\sin\chi)]^2 \tag{20}$$

$$I^{\perp}_{B_{2g}+B_{3g}} \propto \frac{1}{2}\Big\{[e\sin\theta(\sin\varphi\cos^2\chi-\sin\varphi\sin^2\chi+\cos\theta\cos\varphi\sin 2\chi)]^2 + [f\sin\theta(\cos\theta\sin\varphi\sin 2\chi-\cos\varphi\cos 2\chi)]^2\Big\} \quad (21)$$

On the other hand, in the case of a highly crystalline fiber (showing mainly the A_g and B_{3g} modes) with molecular structure almost fully aligned along its long axis, the four above equations can be greatly simplified. Accordingly, one can set periodic dependences only in terms of in-plane rotation angle, χ, in the a-plane of the orthorhombic cell (i.e. according to different polarization geometries), as follows:

$$I^{\parallel}_{A_g} \propto \left|b\cos^2\chi + c\sin^2\chi\right|^2 \quad (22)$$

$$I^{\parallel}_{B_{3g}} \propto |2f\sin\chi\cos\chi|^2 \quad (23)$$

$$I^{\perp}_{A_g} \propto |(b-c)\sin\chi\cos\chi|^2 \quad (24)$$

$$I^{\perp}_{B_{3g}} \propto \left|f\left(\cos^2\chi-\sin^2\chi\right)\right|^2 \quad (25)$$

Note that Eqs. (22) and (25) are only valid for highly aligned structures (e.g. the UHMWPE fiber); in this case, the contribution of the B_{1g} and B_{2g} modes is lost (and, with it, we also lose the possibility of assessing the parameters d and e by using this model sample). However, as far as the fiber sample is concerned, Eqs. (22)–(25) can be used to a degree of precision as trial functions to fit experimental plots of relative intensity of 1170 and 1296 cm^{-1} bands as a function of in-plane rotation angle, χ, as shown in the next section. Fitting of experimental plots obtained in parallel and cross polarization configurations to those periodic functions allows the determination of a set of values for four Raman tensor elements of the orthorhombic structure of UHMWPE (i.e. a, b, c, and f). These values are intrinsic to the orthorhombic cell of UHMWPE; they represent fundamental information for reducing the number of unknown parameters needed in retrieving three-dimensional crystallographic patterns on worn UHMWPE surfaces, for which no guess can be made a priori for orthorhombic lamellae orientation in space.

3.3. Determination of the orientation distribution functions in UHMWPE

The orientation of a polyethylene molecule lying in the Raman probe volume can be expressed in terms of Wigner functions that are reduced to Legendre polynomials after symmetry considerations [19–21,28]. For doing so, an additional set of Euler's angles (α, β, γ) is needed, whose spatial position is relative to a right-handed macroscopic system of Cartesian axes $(xyz)_{lab}$ (cf. Fig. 1b). In our choice, the angle, γ, indicates the degree of anti-clockwise rotation (i.e. about the y_{mol} axis) of the orthorhombic molecular system in the probe volume. The analytical formulation of the probability of finding UHMWPE molecules with orientations between angles (α, β, γ) and ($\alpha+d\alpha$, $\beta+d\beta$, $\gamma+d\gamma$) can be used as a definition for the orientation distribution function, $f(\alpha, \beta, \gamma) \geqslant 0$, as follows:

$$\int_{\gamma=0}^{\gamma=2\pi}\int_{\alpha=0}^{\alpha=2\pi}\int_{\beta=0}^{\beta=\pi} f(\alpha,\beta,\gamma)\sin\beta d\beta d\alpha d\gamma = 1 \quad (26)$$

where $f(\alpha, \beta, \gamma)$ is referred to as the orientation distribution function. Dealing here with in-plane aligned patterns, we shall rule out in first approximation azimuthal dependences and assume that the orientation distribution function is only dependent on the polar angle β (uniaxial symmetry with respect to the y'_{lab} axis).

The resulting orientation distribution function can be in turn expressed as a function of Legendre polynomials, as follows [19]:

$$f(\beta) = \sum_{i=0}^{\infty}\frac{2i+1}{2}\langle P_i(\cos\beta)\rangle P_i(\cos\beta) \quad (27)$$

The coefficients $\langle P_i(cos\beta)\rangle$ are referred to as "order parameters" and should be determined experimentally, while the Legendre polynomials, $P_i(cos\beta)$, of order 2 and 4 are given as:

$$P_2(\cos\beta) = (3\cos^2\beta-1)/2 \quad (28)$$

$$P_4(\cos\beta) = (35\cos^4\beta-30\cos^2\beta+3)/8 \quad (29)$$

By defining an angle, $\beta' = \arctan\left(\frac{\tan\beta}{\tan^2\alpha+1}\right)$ as the angle between the axis y'_{lab} and the projection of the axis y_{mol} onto the plane $(y'z')_{lab}$, it follows that $\theta = \frac{\pi}{2}-\beta'$. Thus, the system of Eqs. (18)–(21) can now be rewritten as follows:

$$I^{\parallel,(\perp)}_{A_g+B_{1g}}(\theta,\varphi,\chi) = \frac{\int_{\gamma=0}^{\gamma=2\pi}\int_{\alpha=0}^{\alpha=2\pi}\int_{\beta=0}^{\beta=\pi} I^{\parallel,(\perp)}_{A_g+B_{1g}}(\beta',\varphi,\chi)f(\beta)\sin\beta d\beta d\alpha d\gamma}{\int_{\gamma=0}^{\gamma=2\pi}\int_{\alpha=0}^{\alpha=2\pi}\int_{\beta=0}^{\beta=\pi} f(\beta)\sin\beta d\beta d\alpha d\gamma} \quad (30)$$

$$I^{\parallel,(\perp)}_{B_{2g}+B_{3g}}(\theta,\varphi,\chi) = \frac{\int_{\gamma=0}^{\gamma=2\pi}\int_{\alpha=0}^{\alpha=2\pi}\int_{\beta=0}^{\beta=\pi} I^{\parallel,(\perp)}_{B_{2g}+B_{3g}}(\beta',\varphi,\chi)f(\beta)\sin\beta d\beta d\alpha d\gamma}{\int_{\gamma=0}^{\gamma=2\pi}\int_{\alpha=0}^{\alpha=2\pi}\int_{\beta=0}^{\beta=\pi} f(\beta)\sin\beta d\beta d\alpha d\gamma} \quad (31)$$

with Raman intensities in the integrals given for the general case by Eqs. (18)–(21) (or by Eqs. (22)–(25) for the highly aligned and crystalline fiber structure). Note that using the equality sign in Eqs. (30) and (31) involves the knowledge of two instrumental constants (i.e. one additive and the other multiplicative to the angular dependences in Eqs. (18)–(25)). Such instrumental constants depend on the optical setup of the spectrometer. The orientation distribution function is then given as:

$$f(\beta) = A\exp[-(\lambda_2 P_2(\cos\beta)+\lambda_4 P_4(\cos\beta))] \quad (32)$$

where A is a constant and the parameters $\lambda_i (i = 2, 4)$ are the Lagrange multipliers used in the definition of the principle of maximum information entropy reported by Jaynes [29]. The three parameters A, λ_2, and λ_4, can be determined by solving the system of three equations given by Eq. (26) and the two equations in the following, which describe the average values of the Legendre polynomials:

$$\langle P_2(\cos\beta)\rangle = \int_{\gamma=0}^{\gamma=2\pi}\int_{\alpha=0}^{\alpha=2\pi}\int_{\beta=0}^{\beta=\pi} P_2(\cos\beta)f(\beta)\sin\beta d\beta d\alpha d\gamma \quad (33)$$

$$\langle P_4(\cos\beta)\rangle = \int_{\gamma=0}^{\gamma=2\pi}\int_{\alpha=0}^{\alpha=2\pi}\int_{\beta=0}^{\beta=\pi} P_4(\cos\beta)f(\beta)\sin\beta d\beta d\alpha d\gamma \quad (34)$$

This system of equations can be solved numerically by applying the trapezoidal rule to the integrals [28].

The order parameter $\langle P_2(cos\beta)\rangle$ is also known as the Herman's orientation parameter [28]. It shall assume the value 0 when the orientation of the orthorhombic lamellae is fully random, while values 1 and −0.5 shall mean a perfect orientation along and perpendicular to a given axis (e.g. the long axis of the fiber), respectively. The Herman's orientation parameter can be considered as the primary parameter to judge the alignment of UHMWPE orthorhombic lamellae [28]. The additional order parameter displayed in the Legendre polynomial, $\langle P_4(cos\beta)\rangle$, also contributes to describing the degree of orientation of the structure. According to a parametric study by Perez et al. [28], the contribution of this latter parameter is less meaningful and straightforward than that of $\langle P_2(cos\beta)\rangle$. For the purpose of this paper, it should suffice to discuss the degree of orientation of the investigated UHMWPE structures by mainly considering the Herman's parameter as an indicator of the degree of orientation of the structure.

4. Results and discussion

4.1. Angular dependence of the A_g and B_{3g} modes and related Raman tensor elements

Fig. 2a and b shows Raman spectra collected on the UHMWPE fiber (calibration) sample as a function of rotation angle, χ in parallel and cross polarization geometry, respectively. As seen, a clear variation in the relative intensity of the 1170 and 1296 cm^{-1} bands can be found by varying the in-plane rotation angle. The experimentally recorded dependence of the relative Raman intensities indeed revealed periodic functions (as shown in Fig. 3a–d for parallel and cross polarization) that could be fitted to a high degree of precision to the trial functions theoretically set in Eqs. (22)–(25) for the selected configurations of the polarization filter. Fitting to trial functions including the orientation distribution (i.e. Eqs. (30) and (31)) was also carried out and showed no appreciable difference in terms of accuracy as compared with fitting to the simplified Eqs. (22)–(25). This is a consequence of the high degree of crystallinity of the fiber, which was found to be as high as $\alpha_c > 99\%$, according to Eq. (2). The Herman's orientation parameter was also determined according to the fitting procedure as $\langle P_2(cos\beta)\rangle = 0.97$, thus confirming the very high degree of axial alignment of the UHMWPE lamellae in the fiber structure. This point will be discussed in comparison with data retrieved on biomedical grades of UHMWPE in Section 4.3. The results of a least-square fitting for the UHMWPE fiber are also shown in Fig. 3a–d for parallel and cross polarization, respectively. In this context, it should be noted that, with applying the angular rotation analysis at a fixed location with n different χ angles in the interval $0 \leqslant \chi \leqslant \frac{\pi}{2}$, one might obtain a system of $4n$ independent equations. When applying Eqs. (30) and (31) to the fiber structure, we come across a total of seven unknown parameters, namely four Raman tensor elements (i.e. a, b, c, and f), one unknown Euler angle, φ, and two order parameters (i.e. $\langle P_2(cos\beta)\rangle$ and $\langle P_4(cos\beta)\rangle$), whose constants A, λ_2 and λ_4 can in turn be obtained according to Eqs. 26, 33, and 34. By considering that two instrumental constants are also involved with the calculation, a total of nine unknown parameters must be determined. It follows that a number of angular assessments $n \geqslant 3$ is needed to retrieve the unknown parameters (i.e. we have made $n = 18$ measurements in the interval $0 \leqslant \chi \leqslant \frac{\pi}{2}$ as shown in Fig. 3(a and b). The fitting procedure led to the determination of values, $a = -0.762$, $b = -0.944$, $c = 0.240$, and $f = 0.622$ for the elements of the Raman tensor. Note that such tensor elements are generally valid parameters for the studied crystal structure, while the other parameters obtained by fitting vary with the measurement location. From the practical side, the availability of the fiber sample enabled us to experimentally calibrate from Raman spectral intensities a set of four Raman tensor element values that represent intrinsic properties of the orthorhombic structure of UHMWPE. The knowledge of such intrinsic parameters greatly reduces the number of unknown parameters to be assessed in setting general equations with the aim of unfolding unknown patterns of local molecular orientation in UHMWPE components (i.e. as shown

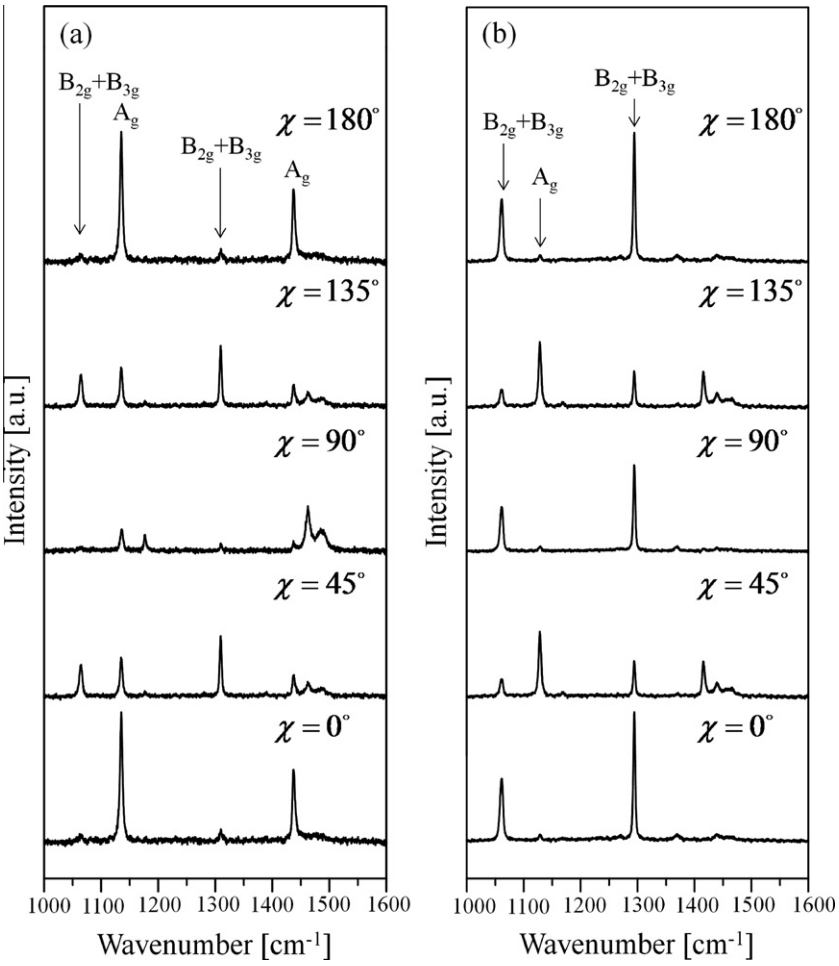

Fig. 2. Raman spectra collected in parallel (a) and cross (b) polarization geometry, as a function of in-plane rotation angle, χ, for the UHMWPE fiber with high degree of crystallinity and molecular alignment. Vibrational modes are labeled on the spectra, according to Table 1.

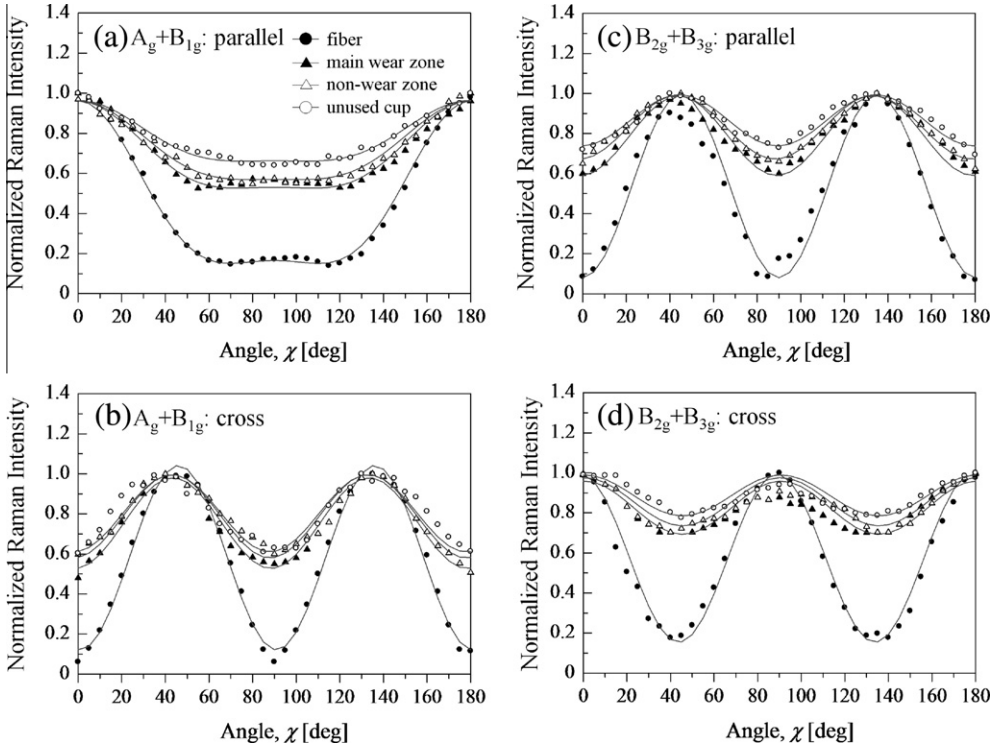

Fig. 3. Experimental plots of the angular dependence of Raman scattering intensities for the orthorhombic structure of UHMWPE. Each plot is representative of Raman spectra averaged over an area of 5×10^4 μm^2. In (a–d), we plotted dependences for parallel and cross polarization modes, respectively. Different symbols are used to represent the fiber sample, the unused acetabular cup and both main wear and non-wear zones in the cup retrieved after 10.3 years (cf. symbols in legend). Lines represent the respective least squares fitting curves obtained with using trial functions as described in the text.

in the following section). We also obtain here a quantitative confirmation about the high crystallinity and the high degree of uniaxial orientation of the UHMWPE fiber sample, which we will then consider as a reference model structure in comparison to the studied UHMWPE biomedical samples.

4.2. Molecular orientation on the surface of retrieved UHMWPE acetabular cups

As a practical application of the Raman polarization technique, we now attempt to visualize the crystallinity and the near-surface molecular orientation in four UHMWPE acetabular cups retrieved after different periods of in vivo exposure, according to a spectral mapping procedure applied to both their main wear and non-wear zones. For comparison, maps were also collected at similar locations in an unused UHMWPE acetabular cup. The fraction of crystallinity was evaluated at each location of the maps according to Eq. (2). On the other hand, a computer program was also set up to calculate the mean molecular orientation of the orthorhombic cell in the Raman probe at each location of the maps and its distribution function (i.e. this latter function is discussed in detail in Section 4.3). Angular in-plane rotation was performed at each location to retrieve both orientation angles and distribution functions according to Eqs. (18)–(21), (30), (and) (31). For solving the above equations, a total of eleven unknown parameters, namely six Raman tensor elements (i.e. *a*, *b*, *c*, *d*, *e*, and *f*), three unknown Euler angles, (θ, φ, χ), and two order parameters (i.e. $\langle P_2(cos\beta)\rangle$ and $\langle P_4(cos\beta)\rangle$), need to be determined (the constants *A*, λ_2 and λ_4 can be obtained from Eqs. 26, 33, and 34). Note that the instrumental constants are now known from experiments on the fiber sample that were performed using the same optical setup. Accordingly, one needs a series of $n \geqslant 3$ angular assessments at each location. Similar to the case of the fiber sample, we performed 18 measurements with different χ angles at each location (as shown in Fig. 3a–d). In the attempt of minimizing the experimental and computational time, we have followed the following procedure. We made a full set of rotation angles at three to five locations (i.e. from 0° to 180° by incremental steps of 5° for a total of 18 Raman spectra for each rotation experiment in the interval $0 \leqslant \chi \leqslant \frac{\pi}{2}$) and run the full computer routine to obtain the full set of Raman tensor elements for the structure. According to these preliminary data, we confirmed the values of *a*, *b*, *c*, and *f* already obtained from the experiments on the UHMWPE fiber and, in addition, we newly retrieved the missing values of −0.403 and −0.849 for the *d* and *e* elements of the Raman tensor, respectively. With the knowledge of the full set of Raman tensor elements, we were then left with five unknown parameters (i.e. three Euler angles and two order parameters) at each location, for whose determination only three Raman spectra per each polarization configuration from different in-plane angles were needed. Figs. 4a–e and 5a–e show typical maps (100×100 μm, in dimension) of crystallinity and molecular orientation patterns, respectively, as collected at the same locations for both wear and non-wear zones. In the above figures, maps in (a), (b), (c), (d), and (e) refer to the unused cup, and to cups retrieved after 2.4, 2.8, 10.3, and 12.2 years, respectively. In the maps of Fig. 5a–e, an orientation of the *c*-axis corresponding to $\chi = 0$ is taken in correspondence of a straight line separating the anterior–superior (A–S) zone of the cup from its posterior–inferior (P–I) zone (i.e. the axis shown in Fig. 5). Positive angles are then counted anti-clockwise. Fig. 6a–e displays histograms of crystallinity, α_c, and of molecular orientation angle, χ, which are representative of the full set of statistical data collected on five 100×100 μm maps per each zone of each cup. The salient features revealed by a comparison among maps and histograms in Figs. 4–6 can be listed as follows:

(i) The statistical trend for the degree of crystallinity in the unused cup was uniformly represented (i.e. over the entire surface of

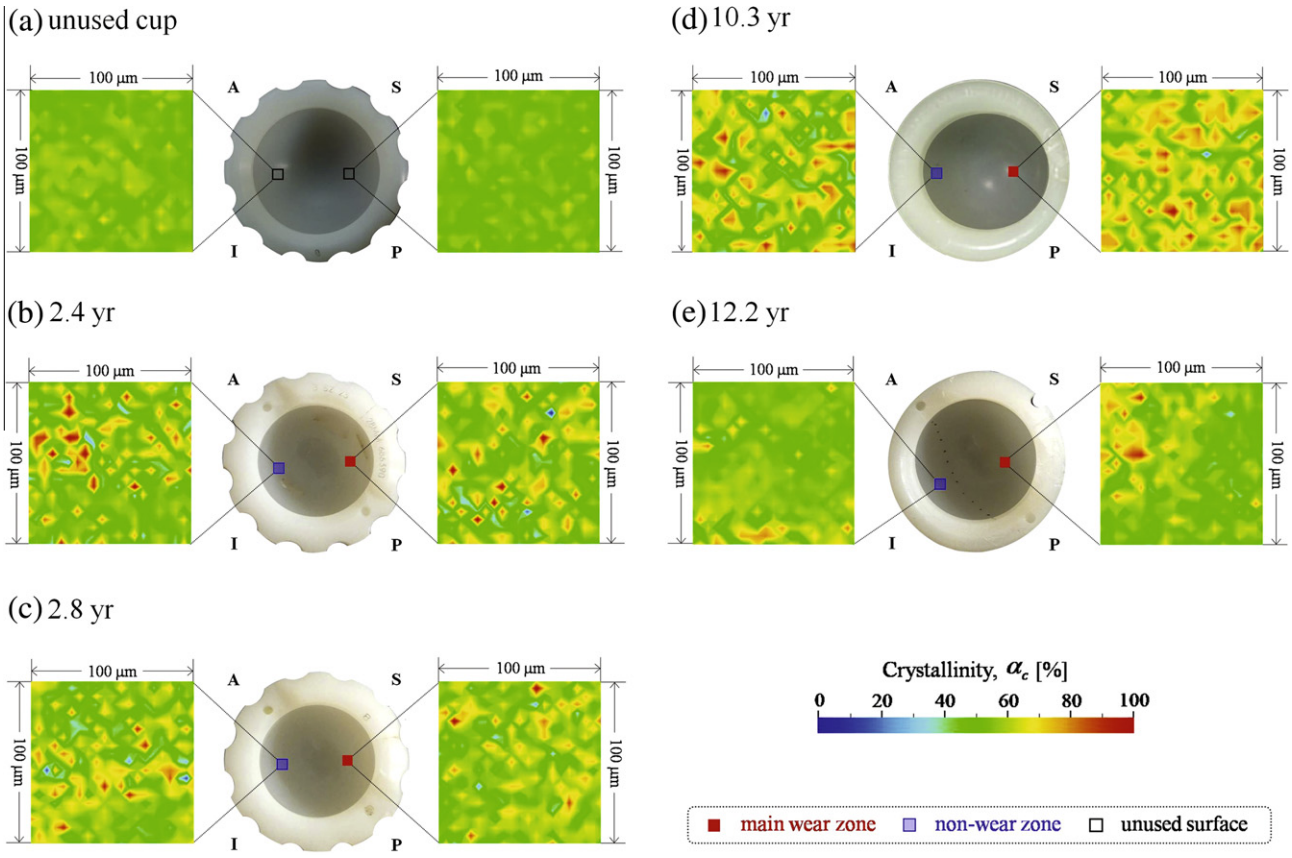

Fig. 4. Typical maps of degree of crystallization, α_c, as revealed by Raman scattering intensities on selected areas of the four investigated retrievals in comparison with the unused acetabular cup. Left and right sides of each retrieved cup are from non-wear and main wear zones, respectively. In analogy, maps were collected at two similar locations also in the unused cup.

the cup) by a relatively broad distribution, whose mean value was determined as about 54%. However, as a general trend, all crystallinity histograms of the in vivo exposed cups appeared to be smeared over a much wider interval of α_c values. As a result, the mean values were only slightly shifted towards higher fractions. Irrespective of exposure time in vivo and of whether they belonged to main wear or non-wear zones, the α_c histograms collected on the bearing surface of the UHMWPE cups appeared significantly altered by in vivo implantation with the formation of "hot spots" of crystallinity reaching values as high as 80–85%.

(ii) The unused cup showed a weak pattern of molecular alignment on its surface, with a quite low value of Herman's parameter, $\langle P_2(cos\beta)\rangle = 0.40$ (cf. histogram in Fig. 6a, Table 2, and the periodical plots of the angular dependence of Raman intensities in Fig. 3a and b in comparison with that of the highly oriented fiber structure). The partial alignment was most likely a consequence of the manufacturing process.

(iii) Unlike the unused cup, the distribution of the in-plane molecular orientation angle, χ, on the surfaces of the retrievals was always bimodal. In other words, the exposure in vivo appeared to introduce a new population of oriented orthorhombic lamellae sharply clustered at orientation angles around 30°. This new angular population grew at the expenses of the originally homogeneous angular population oriented at around 68° as observed in the unused cup. The strongly bimodal character of the angular distribution was a feature common to all maps collected on retrievals as can be easily perceived by the conspicuous absence of grey zones (i.e. the predominance of black and white regions) in the related maps.

(iv) Black regions in the maps of angle, χ, represent the original orientation of the orthorhombic cell on the cup surface after manufacturing. While the distribution of white regions appeared to be random on the analyzed surfaces, the molecular alignment within those zones conspicuously differed from the direction of sliding displacements (gait motion) at the contact surface between femoral head and acetabular cup (cf. displacement and *c*-axis orientation directions in Fig. 4) during walking. This is an important feature, which suggests that also secondary motions (e.g. torsions) play an important role on surface molecular alignment. Analyses of local orientation distribution in non-wear zones showed that the black regions maintained quite low values of the Herman's parameter (i.e. in the narrow range $0.4 \leqslant \langle P_2(cos\beta)\rangle \leqslant 0.47$, as in the case of the unexposed material. The low degree of alignment in non-wear zones can be also confirmed by comparing the angular dependences of Raman intensity in these zones with those in the unused cup (cf. Fig. 3a and b). Interestingly, as far as main wear zones were concerned, white regions in the χ maps often (but not necessarily) corresponded to highly crystallized regions, while no such relationship could be observed in the non-wear zones, despite also showing some increase in degree of crystallinity as compared to the unused cup. In the main wear zones the angular dependences of Raman intensity were more pronounced (cf. Fig. 3a and b) and white areas in the χ maps could locally reach $\langle P_2(cos\beta)\rangle$ values as high as 0.90.

(v) No clear trends for an increase in both crystallinity and Herman's parameter as a function of in vivo exposure time could be obtained in this study. In particular, the long-term retrieval in Figs. 4e and 5e showed significantly lower degrees of crystallinity and molecular alignment as compared with the other long-term retrieval in Figs. 4d and 5d. The values were comparable with those of the short-term exposed cups. While a lack of statistics hampers

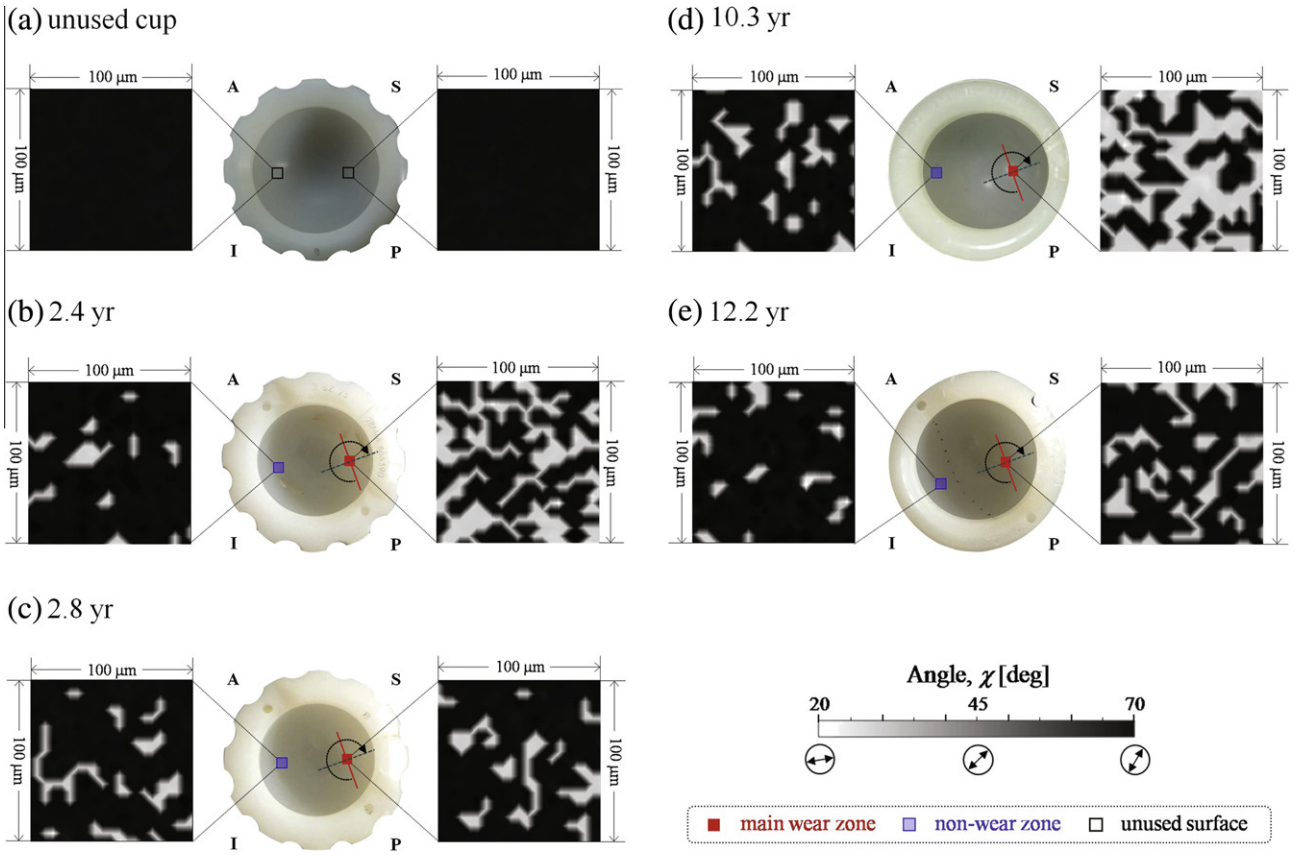

Fig. 5. Typical maps of molecular orientation patterns as revealed by polarized Raman scattering intensities on selected areas of the four investigated retrievals in comparison with the unused acetabular cup. Left and right sides of the maps in the retrieved cups are from non-wear and main wear zones, respectively. In analogy, maps were collected at two similar locations also in the unused cup. Full and broken lines drawn on each retrieved cup represent the approximate direction of gait motion and the mean molecular orientation direction detected in the white areas of the maps, respectively. The arrowed rotation indicates a secondary displacement by torsion that might be at the origin of the observed molecular alignment.

any final conclusion regarding the relationship between the degree of crystallinity/alignment and in vivo exposure time, we can only speculate here that the presumed lower activity of a 60 year old female patient vs. that of a 49 year old male patient could be, for otherwise exactly the same type and size of implant, the reason for the observed structural differences.

Despite such a lack in statistics, the experimental data clearly suggest that the observed variation of structural patterns in the main wear zone, namely both the fractional increase of orthorhombic lamellae population and their clustering around an orientation different from the direction of gait motion in the hip joint, visualizes the occurrence of wear damage on the UHMWPE bearing surface. In other words, the highly crystallized/aligned zones (i.e. the "hot spots" observed in the α_c maps) are formed as a result of prolonged and repetitive sliding motion of the femoral head along the direction of gait motion and are likely to detach from the surface, thus becoming wear debris (in agreement with the phenomenological description given in previous literature [30]). A full description of the depth along the sample subsurface to which such a structural changes might occur in vivo is beyond the scope of this paper and will be the subject of a forthcoming paper. However, preliminary data obtained by shifting the focal plane of the confocal probe along the sub-surface of the acetabular cups (i.e. with steps of 1 μm) revealed detectable spectral variations (i.e. toward the original structure of the unexposed material), starting from a depth $z_0 = 5–8$ μm, while the full restoration of the original structure occurred from depths at around 20 μm.

4.3. Degree of alignment on the surface of retrieved UHMWPE acetabular cups

Average orientation distribution functions, as obtained for the non-wear and main wear zones of the long-term retrieval in Figs. 4d and 5d and the short-term retrieval in Figs. 4c and 5c, are plotted in Fig. 7. For comparison, the functions retrieved for the fiber sample and for the unused cup are also shown as an upper and lower boundary for the degree of orientation of a UHMWPE structure, respectively. All the parameters characterizing the orientation distribution functions are explicitly listed in Table 2. The plots in Fig. 7 are representative of about 2200 spectra over a total area of $\approx 10^5$ μm^2 per each zone of the investigated cup. The degree of alignment can be clearly visualized by the narrow peak centered at $\beta = 0$; the higher the peak the higher the degree of alignment. Results confirm that the probability of finding UHMWPE lamellae oriented along the direction of gait motion in the hip joint was the highest in the main wear zone of the cup sample exposed for a long time in vivo, although such a degree of orientation was far from reaching the extremely high value found for the UHMWPE fiber along its long axis. On the other hand, some increase in the degree of alignment was visible upon exposure in vivo even in the conspicuous lack of mechanical load (i.e. in the non-wear zone), as compared with the unused cup (i.e. $\langle P_2(cos\beta)\rangle = 0.58$ vs. 0.40).

From a general perspective, the present structural analysis by Raman spectroscopy confirms and quantifies how the degree of alignment of the orthorhombic structure on the surface of in vivo exposed UHMWPE acetabular cups depends on loading history,

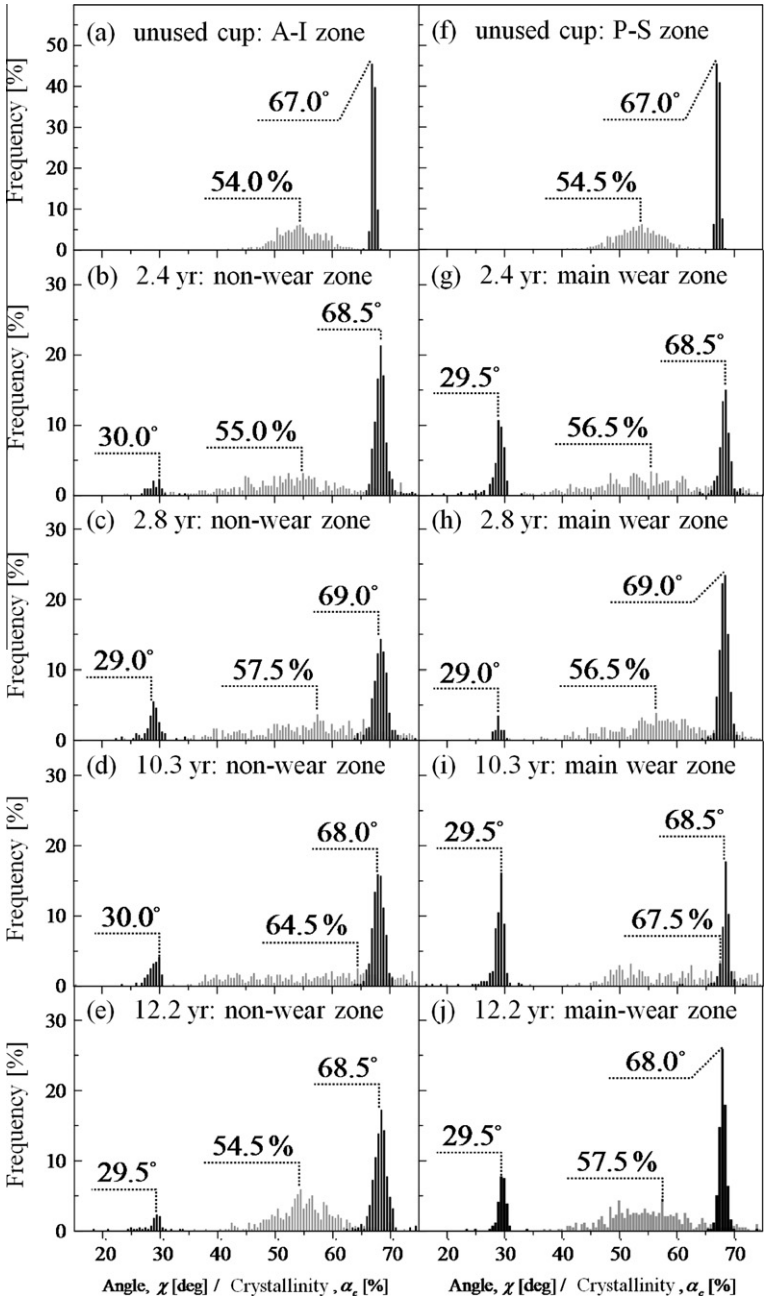

Fig. 6. Histograms of the degree of crystallinity, α_c, and of *c*-axis orientation angle, χ, for both main and non-wear zones of short-term and long-term retrievals as compared with the as-manufactured material. Note the homogeneous structure of this latter sample in both anteroinferior and posterosuperior zones (in (a) and (f), respectively). Each histogram is representative of a surface area of 5×10^4 μm^2.

Table 2
Numerical parameters characterizing the orientation distribution functions plotted in Fig. 7.

Sample	$\langle P_2(cos\beta)\rangle$	$\langle P_4(cos\beta)\rangle$	A	λ_2	λ_4
Fiber	0.97	0.92	3.29×10^{-9}	−10.00	−10.00
Main wear zone <long-term>	0.88	0.78	7.51×10^{-4}	−1.70	−5.00
Main wear zone <short-term>	0.73	0.60	3.18×10^{-3}	−1.65	−3.00
Non-wear zone	0.58	0.44	5.94×10^{-3}	−1.50	−2.00
Unused cup	0.40	0.19	9.10×10^{-3}	−1.50	−0.65

and thus suggests that the Herman's parameter can be seen as a measure of both cumulative wear history and effective lifetime in acetabular cups exposed in vivo.

5. Conclusion

Polarized Raman spectroscopy represents a powerful non-contact technique for the characterization of surface orientation patterns in unused and retrieved acetabular cups made of UHMWPE. In this paper, we explicitly worked out the Raman selection rules and experimentally calibrated the full set of elements of the Raman tensor for the orthorhombic structure of UHMWPE. This body of physical information and properties has been then applied to the quantitative crystallographic assessment of *c*-axis orientation of the orthorhombic cell on the surface of either freshly manufactured or retrieved UHMWPE acetabular cups after different exposure times in vivo. An effort was made to develop a computational algorithm, incorporating both Raman selection rules and the

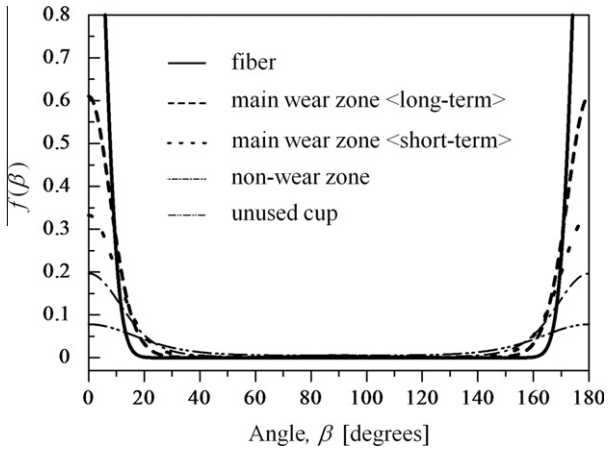

Fig. 7. Orientation distribution functions as calculated from experimental data for the main wear zones of the 10.3-year long-term retrieval and of the 2.8-year short-term retrieval are plotted in comparison with the functions retrieved for the fiber sample and for the unused cup as an upper and lower boundary for the degree of orientation of a UHMWPE structure, respectively. The functions for the non-wear zone between the 10.3- and 2.8-year retrievals in their respective non-wear zone were almost coincident and are represented by the same plot. The ODF function representing the fiber structure is also plotted for reference in the figure. Each function is representative of Raman spectra averaged over an area of 5×10^4 μm^2.

orientation distribution function, for the structural analysis of UHMWPE. This procedure involved an improved analytical approach using Wigner functions expressed in terms of Legendre polynomials. Raman assessments based on this algorithm revealed clear changes in molecular orientation patterns both in main wear and non-wear zones of hip cup retrievals. Although somewhat cumbersome from both experimental and computational viewpoints, the developed Raman methodology provides direct access to the appropriate length scale for quantitative structural assessments in UHMWPE, and thus might give scientists and technologists a chance to experimentally verify the performance and to rationalize the in vivo lifetime of UHMWPE components for biomedical applications.

Acknowledgements

The authors sincerely thank Prof. K. Yamamoto at the Orthopedic Department of Tokyo Medical University for providing the unused and the retrieved acetabular cups examined in this study.

Appendix A. Figures with essential colour discrimination

Certain figures in this article, particularly Figures 1, 4, and 5, are difficult to interpret in black and white. The full colour images can be found in the on-line version, at doi: 10.1016/j.actbio. 2010.02.051.

References

[1] Hozack WJ, Mesa JJ, Carey C, Rothman RH. Relationship between polyethylene wear, pelvic osteolysis and clinical symptomatology in patients with cementless acetabular components. J Arthroplasty 1996;11:769–72.
[2] Campbell P, Ma S, Yeom B. Isolation of predominantly submicron-sized UHMWPE wear particles from periprosthetic tissues. J Biomed Mater Res 1995;29:127–31.
[3] Chenery DH. Detection of peroxy species in ultra-high-molecular-weight polyethylene by Raman spectroscopy. Biomaterials 1997;18:415–9.
[4] Taddei P, Affatato S, Fagnano C, Bordini B, Tinti A, Toni A. Vibrational spectroscopy of ultra-high molecular weight polyethylene hip prostheses: influence of the sterilization method on crystallinity and surface oxidation. J Mol Struct 2002;613:121–9.
[5] Yeom B, Yu Y-J, McKellop HA, Salovey R. Profile of oxidation in irradiated polyethylene. J Polym Sci A Polym Chem 1998;36:329–39.
[6] Fagnano C, Rossi M, Porter RS, Ottani S. A study on solid-state drawn fibers of polyethylene by confocal Raman microspectrometry: evaluation of the orientation profiles of amorphous and crystalline phases across the fiber section. Polymer 2001;42:5871–83.
[7] Ratner S, Moret PM, Wachtel E, Marom G. New Insights into lamellar twisting in transcrystalline polyethylene. Macromol Chem Phys 2005;206:1183–9.
[8] Kyomoto M, Miwa Y, Pezzotti G. Strain in UHMWPE for orthopaedic use studied by Raman microprobe spectroscopy. J Biomater Sci Polym Ed 2007;18(2):165–89.
[9] Kumakura T, Yamamoto K, Puppulin L, Takahashi Y, Pezzotti G. In-depth oxidation and strain profiles in UHMWPE acetabular cups non-destructively studied by confocal Raman microprobe spectroscopy. J Biomater Sci Polymer Ed 2009;20(12):1809–22.
[10] Maxfield J, Stein RS, Chen MC. Polarized Raman studies of crystalline and amorphous orientation in polyethylene. J Polym Sci Polym Phys Ed 1978;16:37–48.
[11] Pigeon M, Prud'homme RE, Pézolet M. Characterization of molecular orientation in polyethylene by Raman spectroscopy. Macromolecules 1991;24:5687–94.
[12] Citra MJ, Chase DB, Ikeda RM, Gardner KH. Molecular orientation of high-density polyethylene fibers characterized by polarized Raman spectroscopy. Macromolecules 1995;28:4007–12.
[13] Nikolaeva GY, Semenova LE, Prokhorov KA, Gordeyev SA. Quantitative characterization of macromolecules orientation in polymers by micro Raman spectroscopy. Laser Phys 1997;7(2):403–15.
[14] Bower DI. Investigation of molecular orientation distributions by polarized Raman scattering and polarized fluorescence. J Polym Sci Polym Phys Ed 1972;10:2135–53.
[15] Frisk S, Ikeda RM, Chase DB, Rabolt JF. Determination of the molecular orientation of poly(propylene terephthalate) fibers using polarized Raman spectroscopy: a comparison of methods. Appl Spectrosc 2004;58(3):279–86.
[16] Minn M, Sinha SK. Molecular orientation, crystallinity, and topographical changes in sliding and their frictional effects for UHMWPE film. Tribol Lett 2009;34:133–40.
[17] Heo SJ, Jang I, Barry PR, Phillpot SR, Perry SS, Sawyer WG, et al. Effect of the sliding orientation on the tribological properties of polyethylene in molecular dynamics simulations. J Appl Phys 2008;103:083502–6.
[18] Sambasivan S, Fischer DA, Shen MC, Hsu SM. Molecular orientation of ultrahigh molecular weight polyethylene induced by various sliding motions. J Biomed Mater Res 2004;70(2):273–85.
[19] Gurp MV. The use of rotation matrices in the mathematical description of molecular orientations in polymers. Colloid Polym Sci 1995;273:607–25.
[20] Bower DI. Orientation distribution functions for biaxially oriented polymers. Polymer 1982;23:1251–5.
[21] McBrierty VJ. Use of rotation operators in the general description of polymer properties. J Chem Phys 1974;61(3):872–82.
[22] Riekel C, Cedola A, Heidelbach F, Wagner K. Microdriffraction experiments on single polymeric fibers by synchrotron radiation. Macromolecules 1997;30:1033–7.
[23] Pezzotti G, Kumakura T, Yamada K, Tateiwa T, Puppulin L, Zhu W, et al. Confocal Raman spectroscopic analysis of cross-linked ultra-high molecular weight polyethylene for application in artificial hip joints. J Biomed Opt 2007;12(1):014011–4.
[24] Lipkin DM, Clarke DR. Sample-probe interactions in spectroscopy: sampling microscopic property gradients. J Appl Phys 1995;77:1855–63.
[25] Mutter R, Stille W, Strobl G. Transition regions and surface melting in partially crystalline polyethylene: a Raman spectroscopic study. J Polym Sci B Polym Phys 1993;31:99–105.
[26] Loudon R. The Raman effect in crystals. Adv Phys 1964;13:423–82.
[27] Porto SP, Krishnan RS. Raman effect of corundum. J Chem Phys 1967;47:1009–12.
[28] Pérez R, Banda S, Ounaies Z. Determination of the orientation distribution function in aligned single wall nanotube polymer nanocomposites by polarized Raman spectroscopy. J Appl Phys 2008;103:074302.
[29] Jaynes ET. Information theory and statistical mechanics. Phys Rev 1957;106:620–30.
[30] Kabo JM, Gebhard JS, Loren G, Amstutz HC. In-vivo wear of polyethylene acetabular components. J Bone Joint Surg Br 1993;75:254–8.